IEEE Access
Multidisciplinary | Rapid Review | Open Access Journal

Received January 14, 2019, accepted January 23, 2019, date of publication January 29, 2019, date of current version February 14, 2019.

Digital Object Identifier 10.1109/ACCESS.2019.2895740

Low-Profile ESPAR Antenna for RSS-Based DoA Estimation in IoT Applications

MATEUSZ BURTOWY, MATEUSZ RZYMOWSKI, AND LUKASZ KULAS, (Senior Member, IEEE)
Department of Microwave and Antenna Engineering, Faculty of Electronics, Telecommunications and Informatics, Gdańsk University of Technology, 80-233 Gdańsk, Poland

Corresponding author: Lukasz Kulas (lukasz.kulas@pg.edu.pl)

This work was supported in part by the SCOTT Project through the Electronic Component Systems for European Leadership Joint Undertaking under Grant 737422, and in part by the European Union's Horizon 2020 Research and Innovation Programme and Austria, Spain, Finland, Ireland, Sweden, Germany, Poland, Portugal, Netherlands, Belgium, and Norway.

ABSTRACT In this paper, we have introduced a low-profile electronically steerable parasitic array radiator (ESPAR) antenna that can successfully be used to estimate the direction-of-arrival (DoA) of incoming signals in wireless sensor network (WSN) applications, in which the height of the complete antenna has to be low. The proposed antenna is over three times lower than high-profile ESPAR antenna designs currently available in the literature for the DoA estimation; it can provide eight unique main beam directions and relies on simplified beam steering, which makes it applicable to simple and inexpensive WSN nodes. Measurements using our fabricated ESPAR antenna prototype indicate that relying solely on the received signal strength values recorded at the antenna output port, it is possible to achieve accurate DoA estimation results with error levels similar to those available for high-profile ESPAR antennas relying on the similar energy-efficient simplified beam steering concept and having 12 unique main beam directions. As a consequence, the overall time required for the DoA estimation using the proposed antenna can be reduced by 33%.

INDEX TERMS Switched-beam antenna, electronically steerable parasitic array radiator (ESPAR) antenna, direction-of-arrival (DoA), received signal strength (RSS), Internet of Things (IoT), smart city.

I. INTRODUCTION

Internet of Things (IoT) is one of the key technologies supporting developments of Smart City applications, as it provides inexpensive, unified, and simple access to physical elements within city infrastructure [1], [2]. In such systems, relying mostly on wireless sensor network (WSN) installations, energy shortage together with connectivity problems are among the most important factors limiting the number of IoT deployments [3]. This problem is particularly pronounced in smart parking and smart building applications having clear return of investment [1], in which IoT gateways and sensors have to be attached to the ceiling, placed on the street or even buried under the asphalt [1]–[3]. Measurements conducted within installations in SmartSantander testbed indicate, that although IEEE 802.15.4 standard can be considered as very practical in most of the cases, connectivity problems tend to appear in parking applications [3] when the system operates in real weather and traffic conditions. One of the possible solutions, verified experimentally in real smart city testbed, is to use antennas with higher antenna gains. After installing antennas having 5 *dBi* gain, communication between WSN gateways and IoT nodes improved considerably [3]. However, in such approach, the most optimal antenna directions have to be set manually during the installation process, and once fixed they cannot easily be modified afterwards.

To overcome connectivity problems in IoT-based systems, electronically steerable parasitic array radiator (ESPAR) antennas can be integrated within WSN nodes and gateways [4]. ESPAR antenna is a promising concept that allows one to form antenna beam and change associated radiation direction electronically based on the theory introduced by Harrington [5]. Such antennas have only a single active element, which is surrounded by a number of passive elements being connected to variable reactances [6]–[8]. The radiation pattern can be then formed by setting such reactances to appropriate values and, additionally, by changing these values electronically [6], it can also easily be rotated around the active element [6], [8].

ESPAR antennas may be used as an alternative cost-effective solution to estimate direction-of-arrival (DoA) of

The associate editor coordinating the review of this manuscript and approving it for publication was Wei Liu.

incoming signals. Instead of using a number of digital signal processing (DSP) units together with antennas forming an array, which provide highly accurate results when algorithms like MUltiple SIgnal Classification (MUSIC) are used, it is possible to find DoA angles by rotating ESPAR antenna main beam electronically, while incoming signal samples are being recorded [8], [9] at a single output. Using such approach, one can estimate DoA of a signal impinging the antenna with 2° precision using power pattern cross-correlation (PPCC) algorithm introduced in [10]. Moreover, because PPCC method relies on recorded received signal strength (RSS) values only, it has been possible to adapt ESPAR antenna design to wireless sensor network (WSN) nodes by simplifying beam steering circuit [8], [11]. In consequence, ESPAR antennas together with PPCC method can enable DoA estimation functionality in WSN nodes equipped usually with small and inexpensive radio frequency (RF) transceivers that can measure RSS values of received packets, but not having DSP processing capability. One should note, however, that, due to main beam switching required in ESPAR-based approach, the time required to produce DoA estimation results will be longer than in array-based DSP approach.

Cost-effective and energy-efficient WSN nodes having DoA estimation functionality can improve connectivity, coverage and energy efficiency of the whole network [12]–[14]. They can also be used to develop scalable and low-cost indoor localization systems in the 2.4 *GHz* industrial, scientific and medical (ISM) RF band [15], which are able to support smart building or smart hospital applications that rely on real-time positions of assets or people [16]. However, in some cases, it is required that WSN base stations mounted in the building or on the car should have the lowest profile possible [16]–[17], which is not the case in the original ESPAR antenna concepts.

Low-profile ESPAR antennas, which have linear polarization aligned with the original design proposed in [10], are already available in the literature to address different application areas [17]–[26]. These areas involve DoA estimation based on MUSIC algorithm [17], jamming mitigation [18] or beam switching [19]–[26]. However, in order to provide accurate RSS-based DoA estimation for low-cost WSN nodes equipped with inexpensive RF transceivers and microcontrollers, one has to provide ESPAR antenna design that involve at least 6 unique main beam directions with radiation patterns having monotonic drop from the maximum and low side lobe level (SLL) [10], [27]. These conditions are not fulfilled by the low-profile ESPAR antenna designs available in [17]–[26].

In this paper, a new low-profile ESPAR antenna with simplified beam steering, which is designed for accurate RSS-based DoA estimation in WSN, is proposed. The antenna can provide 8 unique main beam directions and can easily be integrated within WSN nodes equipped with an inexpensive radio transceiver. Measurement results involving PPCC-based DoA estimation indicate that the proposed design provide the overall accuracy at the similar level as in the case of high-profile ESPAR antenna with simplified beam steering and 12 unique main beam directions [10], [11], [27]. Therefore, DoA estimation performed by a WSN node equipped with our low-profile ESPAR antenna can be performed 33% faster. Additionally, we show that the proposed antenna can successfully be used in demanding Smart City installations, in which signal-to-noise ratio (SNR) is low.

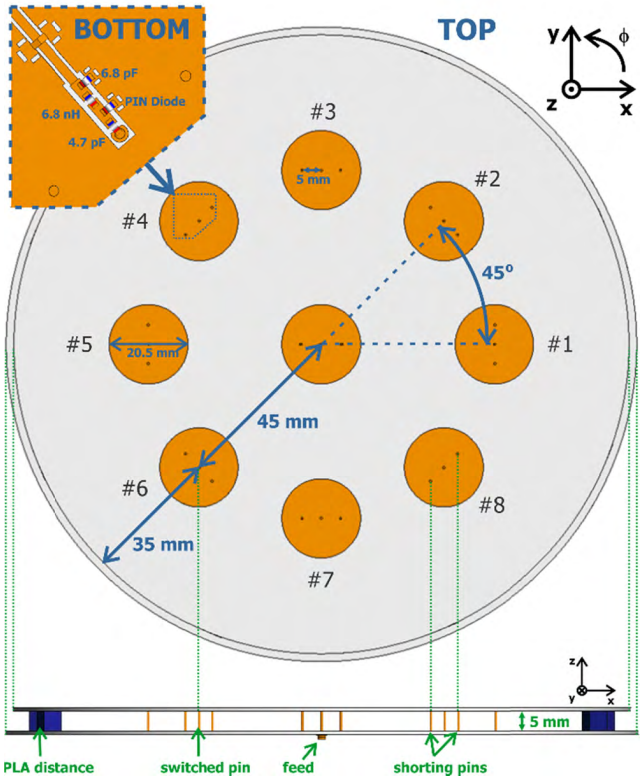

FIGURE 1. Designed low-profile ESPAR antenna together with numbering of its passive elements. All the dimensions are in millimeters.

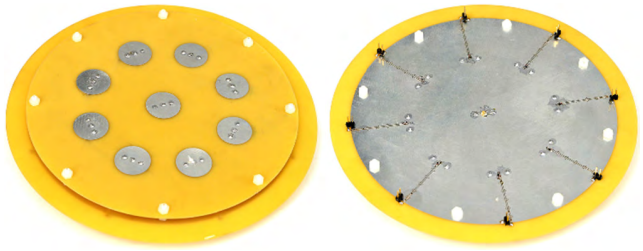

FIGURE 2. Realized low-profile ESPAR antenna: top with visible circular radiating elements and bottom that contains pin-based steering circuits.

II. ANTENNA DESIGN AND REALIZATION

The proposed antenna, shown in Fig. 1 and Fig. 2, consists of two substrate layers, separated by an air gap. The top layer with nine loaded-disk microstrip radiators is located over the bottom layer where the groundplane and switching circuits have been placed. In the design, similar to original ESPAR antenna concepts [6], [7], the central radiating element, fed by coaxial connector via the central pin, is surrounded by

eight passive elements that can modify the antenna radiation pattern when proper loads are connected. Both layers were realized using 0.95 *mm* height FR4 substrate with $\varepsilon_r = 4.4$, so the antenna can be used in inexpensive WSN nodes.

To design low-profile ESPAR antenna that has significantly reduced height when compared to the original concepts [6], [7], while its radiation patterns can successfully be used to provide accurate DoA estimation, a number of constructions based on microstrip radiators has been investigated [28], [30], [32], [33]. To this end, each disk radiator is loaded with two shorting pins, permanently connected to the antenna groundplane. The shorting pins are often used for the antenna input impedance matching [34] as they introduce additional inductance, influence the operational bandwidth and reduce the patch size what leads to greater number of switching configurations when elements are formed in an array within a constrained PCB area. The main factor that affects the substrate effective permittivity is the airgap between the radiation layer and groundplane. As it lowers the effective permittivity and increases the height of the substrate, the resonant frequencies of various modes will increase as well as the operational bandwidth [35]–[38].

The central pin of every surrounding passive element can be connected to the ground via a corresponding switching circuit realized using SMP1320-040LF PIN diode, which is shown in Fig. 1. Therefore, the switching mechanism influence the passive elements' resonance by involving additional, centrally located load (close to open or short circuit). In such structure, TM01 dominant mode is excited, which results in antenna radiation pattern having shape of the conical beam [28], similar to the dipole antenna. As a consequence, the proposed antenna provides 360° beam steering with 45° discrete step using $N = 8$ directional radiation patterns. In such setup, nth radiation pattern will have its main beam direction equal to φ^n_{max}, for which the radiation pattern will have its maximum in the horizontal plane. In consequence, antenna's configuration can be denoted by the corresponding steering vector $V^n_{max} = [v_1 v_2 \cdots v_s \cdots v_8]$, where v_s denotes the state of each passive disk's switching circuit: $v_s = 1$ for sth passive radiator connected via corresponding switched pin to the ground and 0 for opened. All considered steering vectors together with associated main beam directions and radiation pattern numbers are gathered in table 1, in which the first radiation pattern have the main beam direction at $\varphi^1_{max} = 0°$ (aligned with x axis in Fig. 1) and is created using steering vector $V^1_{max} = [1\ 1\ 0\ 0\ 0\ 0\ 0\ 1]$.

The proposed structure has been designed and optimized in Altair FEKO simulator at the center frequency 2.45 *GHz* to provide the narrowest directional beam with low SLL in the horizontal plane, which was possible for three consecutive passive elements shorten to the ground. From the resulting dimensions in Fig. 1, one can easily notice that the total antenna height is 6.9 *mm* that is significantly lower than the height of traditional ESPAR antennas presented in [8] and [10], which equals 30.17 *mm* and 57.93 *mm* respectively. The complete manufactured antenna prototype

TABLE 1. Antenna's main beam directions for different steering vectors applied to the designed low-profile ESPAR antenna (see text for explanations).

n	V^n_{max}	φ^n_{max}
1	11000001	0°
2	11100000	45°
3	01110000	90°
4	00111000	135°
5	00011100	180°
6	00001110	225°
7	00000111	270°
8	10000011	315°

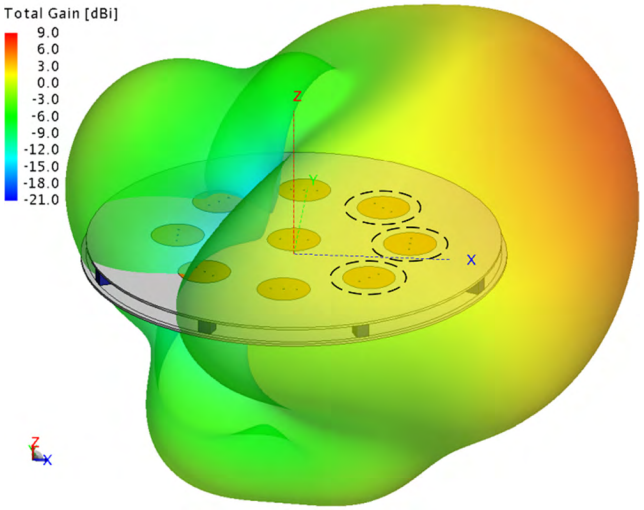

FIGURE 3. Simulated 3D radiation pattern of the proposed antenna at 2.484 GHz for the steering vector V^1_{max} = [11000001] with passive elements shorten to the ground marked by a black dashed circle lines (see text for explanations).

together with switching circuit, which is shown in Fig. 2, has a total height equal to 10 *mm*. Moreover, we have removed ground skirt present in the first ESPAR antenna publications [6], [7], [10], so the resulting radiation pattern of the proposed antenna, shown in Fig. 3, is much wider in elevation direction than in the original ESPAR antenna designs [8], [10], which will improve WSN connectivity in scenarios when there is a difference in height of installed WSN nodes [15], [16], [39], [40].

Antenna measurement results, shown in Fig. 4 and Fig. 5, indicate that the antenna provides 8 directional radiation patterns by providing proper steering vectors. As the structure is not fully symmetrical, we have carefully inspected three configurations having the most asymmetrical orientation with respect to the central element. The results presented in Fig. 4, Fig. 5 and in table 2 show that the asymmetry has a minor impact on the antenna parameters influencing DoA estimation accuracy the most [27]: HPBW and SLL differences in the horizontal plane (i.e. $\theta = 90°$) for each configuration are less than 3° and 1.8 *dB* respectively. Additionally, there is a good match between measured antenna gains and input impedance matching levels, which for all configurations are

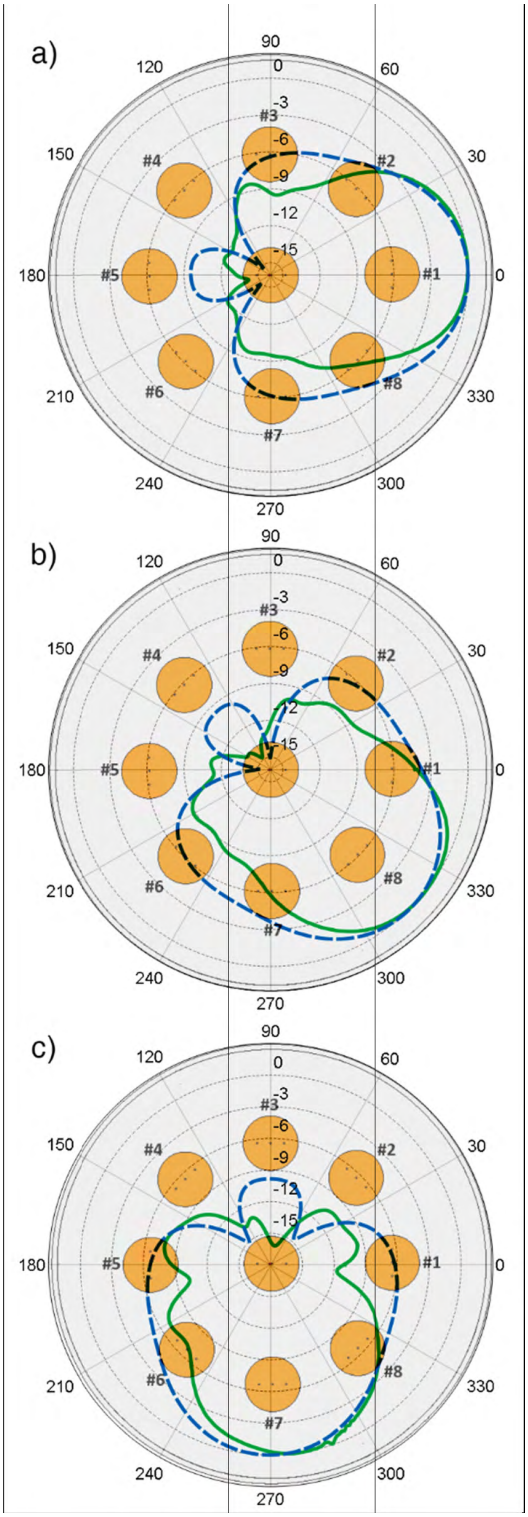

FIGURE 4. Simulated (blue dashed line) and measured (green solid line) normalized radiation patterns of E_θ field component at 2.484 GHz in the horizontal plane with respect to the central active element for three different configurations of the proposed antenna: a) V^1_{max} = [11000001], b) V^8_{max} = [10000011], c) V^7_{max} = [00000111] (see text for explanations).

below -10 dB in the considered frequency band, and the antenna provides gain values sufficient for IoT-based Smart City deployments [3].

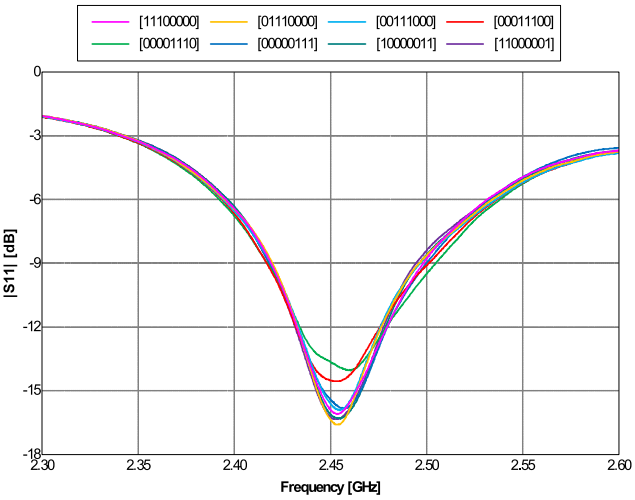

FIGURE 5. Input impedance matching measured for all considered configurations of the proposed antenna expressed by the corresponding steering vectors in the legend.

TABLE 2. Measured parameters of the realized antenna for three configurations at 2.484 GHz (see text for explanations).

	V^1_{max} = [11000001]	V^8_{max} = [10000011]	V^7_{max} = [00000111]
φ_{max} [°]	0	315	270
HPBW @θ=90 [°]	69.1	67.7	66.2
SLL @θ=90 [dB]	7.0	8.4	8.8
Gain @θ=90 [dBi]	4.7	4.4	4.2
Max Gain [dBi]	7.5	7.3	7.5
|S11| [dB]	-10.6	-10.9	-11.2

III. RSS-BASED DIRECTION-OF-ARRIVAL ESTIMATION FOR INTERNET OF THINGS APPLICATIONS

In order to perform RSS-based DoA estimation accurately using the proposed low-profile ESPAR antenna, one can implement power pattern cross-correlation (PPCC) algorithm. It relies on the cross-correlation coefficient originally introduced in [10], which, after adaptation to simplified beam steering concept [8] and the proposed antenna, can be written in the following vector form [11]:

$$g = \frac{\sum_{n=1}^{8} \left(\boldsymbol{p}^n Y\left(V^n_{max}\right)\right)}{\sqrt{\sum_{n=1}^{8} \left(\boldsymbol{p}^n \circ \boldsymbol{p}^n\right)} \sqrt{\sum_{n=1}^{8} Y\left(V^n_{max}\right)^2}} \tag{1}$$

where $\boldsymbol{p}^1, \boldsymbol{p}^2, \ldots, \boldsymbol{p}^8$ are the antenna's radiation pattern values measured for all the corresponding steering vectors $\left\{V^1_{max}, V^2_{max}, \ldots, V^8_{max}\right\}$ in an anechoic chamber once with the angular step precision $\Delta\varphi$ during calibration phase prior to the actual DoA measurements, $Y\left(V^1_{max}\right), Y\left(V^2_{max}\right), \ldots, Y\left(V^8_{max}\right)$ are output power values recorded for a signal impinging the antenna from an unknown direction during the on-line phase and the symbol '$\circ$' stands for the Hadamard product, which is element-wise product of vectors. Because vectors $\boldsymbol{p}^n = \left[p^n_1, p^n_2, \cdots, p^n_I\right]^T$ contain discretized radiation pattern values corresponding to discretized

horizontal angles $\boldsymbol{\varphi} = [\varphi_1, \varphi_2, \cdots, \varphi_I]^T$, the resulting vector $\boldsymbol{g}$ of length I will contain discretized values of PPCC cross-correlation coefficient [10], [11] associated with the values in $\boldsymbol{\varphi}$ as well. In consequence, by finding a value in the vector $\boldsymbol{\varphi}$ corresponding to the highest value of $\boldsymbol{g}$, one will simultaneously determine the estimated DoA angle $\hat{\varphi}$ [8], [10], [11].

In practical IoT deployment scenarios, height differences may be present between WSN gateways, installed as a part of Smart City wireless communication infrastructure, and IoT nodes installed within the environment. When such differences are comparable or greater than distances among them, which is usually the case in smart parking or smart building applications [3], inaccurate DoA results for elevation angles different than those close to the horizontal plane [39], [40] may be produced using (1). To overcome this effect and to provide accurate DoA estimations for arbitrary elevation angles, one can implement PPCC algorithm involving multiple calibration planes (MCP) measured along the elevation plane. For the proposed antenna, PPCC-MCP estimator that has been introduced in [40] can be written in the following vector form:

$$\boldsymbol{g}_\theta = \frac{\sum_{n=1}^{8} \left(\boldsymbol{p}_\theta^n Y\left(V_{max}^n\right)\right)}{\sqrt{\sum_{n=1}^{8} \left(\boldsymbol{p}_\theta^n \circ \boldsymbol{p}_\theta^n\right)} \sqrt{\sum_{n=1}^{8} Y\left(V_{max}^n\right)^2}} \tag{2}$$

where $\boldsymbol{g}_\theta$ contains PPCC-MCP cross-correlation coefficient in a vector form, while vectors $\boldsymbol{p}_\theta^n$ contain ESPAR antenna's radiation pattern values measured at angles θ_m for every considered steering vector V_{max}^n and can be written as:

$$\boldsymbol{p}_\theta^n = \left[\left(\boldsymbol{p}_{\theta_1}^n\right)^T, \left(\boldsymbol{p}_{\theta_2}^n\right)^T, \cdots, \left(\boldsymbol{p}_{\theta_M}^n\right)^T\right]^T \tag{3}$$

When M calibration planes $\{\theta_1, \theta_2, \ldots, \theta_M\}$ are considered, the length of the vector $\boldsymbol{p}_\theta^n$ is equal to $I * M$. Discretized radiation pattern values within $\boldsymbol{p}_\theta^n$ correspond to discretized values of φ in the following vector $\boldsymbol{\varphi}_\theta$:

$$\boldsymbol{\varphi}_\theta = \left[\boldsymbol{\varphi}_{\theta_1}^T, \boldsymbol{\varphi}_{\theta_2}^T, \cdots, \boldsymbol{\varphi}_{\theta_M}^T\right]^T, \quad \bigwedge_m \boldsymbol{\varphi}_{\theta_m} = \boldsymbol{\varphi} \tag{4}$$

As a result, $\boldsymbol{g}_\theta$ is also a vector of length $I * M$ corresponding to discretized values of φ in the vector $\boldsymbol{\varphi}_\theta$. Therefore, the estimated DoA angle is a value in the vector $\boldsymbol{\varphi}_\theta$, for which the value in $\boldsymbol{g}_\theta$ is the highest [40].

IV. MEASUREMENTS

To verify DoA estimation performance of the proposed low-profile ESPAR antenna, recently introduced calibration method [31], which allows to determine the overall accuracy of RSS-based DoA estimation schemes employing ESPAR antennas, have been used. The method relies on software-defined radio (SDR) setup, presented in Fig. 6 and Fig. 7, that allows for simultaneous calibration and verification in a fast and reliable way. To this end, all the required ESPAR antenna radiation patterns associated with the eight main beam directions have been measured in our $11.9\,m \times 5.6\,m \times 6.0\,m$ anechoic chamber at $2.484\,GHz$ with the angular step precision $\Delta\varphi = 1°$ and in $M = 9$ calibration planes,

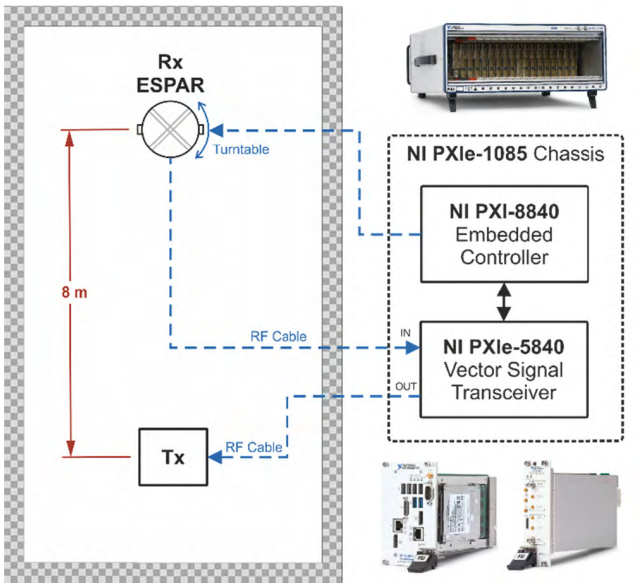

FIGURE 6. The measurement setup installed in our anechoic chamber to conduct the experiment. An SDR-based device (NI PXIe-5840), acting as a signal generator, is sending signals to the transmitting antenna placed on a pole stand. The signals are received by the same device connected to the output of the investigated ESPAR antenna.

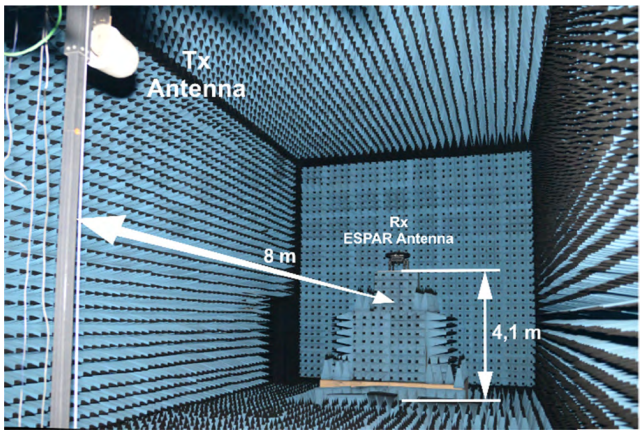

FIGURE 7. The anechoic chamber used in measurements. The ESPAR antenna is placed on a turntable used to set antenna's orientation in both, vertical and horizontal, planes with one degree angular resolution.

namely $\{\theta_1 = 10°, \theta_2 = 20°, \ldots, \theta_9 = 90°\}$, using an SDR-based device (NI PXIe-5840) acting as a signal generator and a signal analyzer. For each angular measurement during the calibration phase, 100 sinusoidal snapshots were sent from the transmitting antenna placed on a pole stand at $H = 4.1\,m$, 8 meters from the turntable, on which the proposed antenna was mounted, and then the signal was received and averaged at the antenna output port. As a result, $I = 360$ calibration points were produced for every elevation plane.

To examine DoA estimation accuracy, 10 snapshots of 10 dBm 2.484 GHz BPSK test signal impinging the proposed low-profile ESPAR antenna were generated in the same anechoic chamber setup for every RSS measurement.

TABLE 3. Summary and comparison of the results obtained for the proposed antenna with the results available in the literature for realized 2.4 GHz ISM RF band antennas.

Parameter [Unit]	[10]	[31]	[17]	[21]	[25]	[26]	This work
Profile [low/ high]	high	high	low	low	low	low	**low**
Height [mm]	57.93	30.17	0.125	0.813	10.6	1.575	**10**
No. of directional radiation patterns	6	12	5	4	4	4	**8**
Steering direction w.r.t. the antenna plane	horizontal	horizontal	vertical	horizontal	horizontal	horizontal	**horizontal**
HPBW in the steering direction [°]	90-100	65-71	*45-93**	120	100 – 140	50-60	**66.2 – 69.1**
Max Gain [dBi]	N/A	*8.31**	5.1	3.5	5.1 - 5.6	7.8	**7.3 - 7.5**
Bandwidth [MHz]	N/A	202	N/A	430	40	*not matched*	**63**
Steering element	varactor diode	SPDT switch	varactor diode	PIN diode	PIN diode	varactor diode	**PIN diode**
Steering method	DSP-based	switching	DSP-based	switching	switching	DSP-based	**switching**
WSN applicable	no	yes	no	yes	yes	no	**yes**
DoA functionality presented	yes	yes	*yes**	no	no	no	**yes**
DoA method	PPCC	PPCC	*MUSIC**	N/A	N/A	N/A	**PPCC**
DoA test data points	36	36	*3**	N/A	N/A	N/A	**36**
DoA test frequency [GHz]	2.484	2.484	*2.4**	N/A	N/A	N/A	**2.484**
SNR [dB]	20	20	*20**	N/A	N/A	N/A	**20**
RMS [°]	0.88	0.61	*1.66**	N/A	N/A	N/A	**0.85**
Precision [°]	2	2	*1.5**	N/A	N/A	N/A	**2**

* *only simulated results are available*

All the signals have been received at the antenna's output and then additive white Gaussian noise has been added to obtain a required signal-to-noise ratio (SNR). To compare results with those already available in the literature, signal's directions were set by rotating the receiving low-profile ESPAR antenna with discrete angular steps equal to $\Delta\varphi_t = 10°$ and $\Delta\theta_t = 10°$ in horizontal and elevation directions respectively. As a result, 36 test directions $\varphi_t \in \{0°, 10°, \ldots, 350°\}$ for 9 elevation angles $\theta_t \in \{90°, 80°, 70°, 60°, 50°, 40°, 30°, 20°, 10°\}$ were generated.

A. DIRECTION-OF-ARRIVAL ESTIMATION USING PPCC ALGORITM

To perform fair comparison of DoA estimation results produced using the proposed low-profile ESPAR antenna with those already available in the literature, the estimated DoA angle has been calculated using power pattern cross-correlation (PPCC) algorithm (1) for the BPSK test signal coming from 36 test directions within the horizontal plane (i.e. $\theta_t = 90°$) and SNR equal to 20 dB. Then, the absolute values of estimation errors were calculated for all the considered horizontal directions $\varphi_t \in \{0°, 10°, \ldots, 350°\}$, which resulted in 36 values shown in Fig. 8, with total root-mean-square (RMS) error equal to 0.85° and 2° precision being the maximum error value.

In table 3 we have gathered obtained accuracy levels together with other relevant parameters of the proposed antenna together with the results already available in the literature. Comparing the obtained results with DoA estimation accuracy levels produced under the same SNR for high-profile ESPAR antenna having 12 unique main beam directions and the same energy-efficient simplified beam steering (0.61° RMS error and 2° precision reported in [31]) and high-profile ESPAR antenna with expensive, both in cost and energy, DSP-based beam steering and having 6 unique main beam directions (0.88° RMS error and 2° precision reported in [10]), we can observe that, although the proposed low-profile antenna can provide only 8 unique main beam directions and relies on simplified beam steering, it provides the same precision as the high-profile ESPAR antennas. One should note, however, that using lower number of unique main beam directions increases the RMS error value when compared to the high-profile ESPAR antenna having 12 unique main beam directions and simplified beam steering.

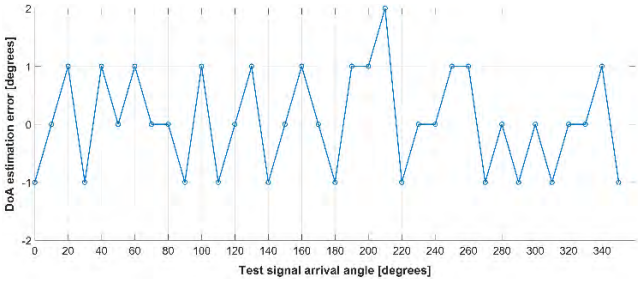

FIGURE 8. DoA estimation error results obtained from the measurements of the proposed low-profile ESPAR antenna in the horizontal plane at SNR=20 dB (see text for explanations).

B. DIRECTION-OF-ARRIVAL ESTIMATION USING PPCC-MCP ALGORITM

Because in the original implementation, PPCC-based DoA estimation relies on calibration measurements in the horizontal plane only (i.e. for $\theta = 90°$), inaccurate results may be produced when θ angle of an unknown incoming signal

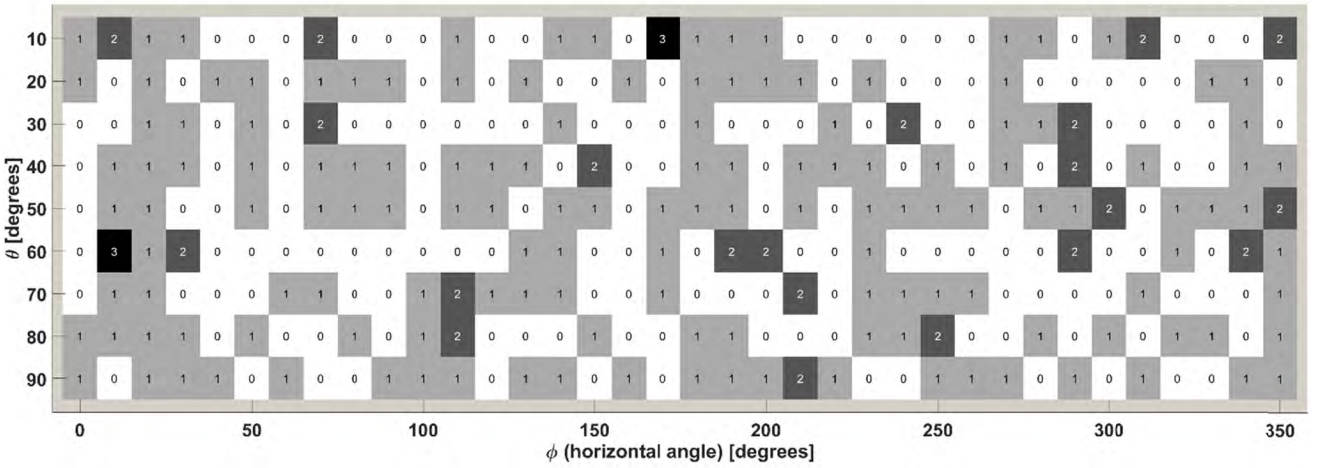

FIGURE 9. Absolute values of DoA estimation errors calculated using PPCC-MCP algorithm for different test angles in horizontal and elevation directions used in the measurements at SNR=20 dB (see text for explanations).

TABLE 4. DoA estimation errors obtained for the proposed low-profile ESPAR antenna and PPCC-MCP algorithm (see text for explanations).

θ_t	SNR = 20 dB		SNR = 10 dB		SNR = 0 dB	
	RMS	prec.	RMS	prec.	RMS	prec.
10°	1.01°	3°	0.93°	2°	2.43°	7°
20°	0.71°	1°	1.03°	2°	2.13°	4°
30°	0.76°	2°	1.19°	2°	2.06°	6°
40°	0.88°	2°	1.05°	3°	2.08°	4°
50°	0.93°	2°	1.31°	3°	2.24°	6°
60°	1.00°	3°	1.54°	4°	2.11°	5°
70°	0.80°	2°	1.29°	3°	2.48°	8°
80°	0.83°	2°	1.24°	3°	2.32°	4°
90°	0.85°	2°	1.32°	4°	2.61°	8°
Cumul.	**0.87°**	**3°**	**1.22°**	**4°**	**2.28°**	**8°**

is different than $\theta = 90°$ [39], [40]. As it may be the case in practical IoT installations, PPCC algorithm involving multiple calibration planes (MCP) is used to overcome this effect [40].

To verify DoA estimation accuracy results obtained using the proposed low-profile ESPAR antenna and PPCC-MCP method, calibration results produced in $M = 9$ calibration planes, namely $\{\theta_1 = 10°, \theta_2 = 20°, \ldots, \theta_9 = 90°\}$, having $\Delta\varphi = 1°$ precision in the horizontal direction were used, which resulted in $\boldsymbol{p}_\theta^n$ vectors of the length equal to $360 * 9$. Estimated DoA angles were calculated using PPCC-MPC algorithm (2) for a BPSK test signal coming from 36 test horizontal directions ($\varphi_t \in \{0°, 10°, \ldots, 350°\}$) within 9 elevation planes for three considered SNR values. Results gathered in Fig. 9 and summarized in table 4 indicate that the proposed low-profile ESPAR antenna will provide accurate DoA estimation results for all elevation angles. Moreover, it generates acceptable values also for low SNR levels, which can be the case in practical Smart City installations relying on inexpensive IoT nodes installed in interference-rich propagation environments.

It is worth noticing that, although the radiation patterns gradually lose their directional character for decreased θ angles [39], [40], it can be observed in Fig. 9 that, due to calibration method used within PPCC-MCP algorithm, DoA estimation results do not deteriorate significantly for low θ values when SNR equals to 20 dB. However, DoA estimation results for lower SNR values presented in table 4 show deterioration not only for low θ angles, but also for higher ones. Therefore, to assess the overall DoA estimation accuracy for PPCC-MCP algorithm one should rely on cumulative RMS and precision values, which are calculated for all considered test directions.

C. DIRECTION-OF-ARRIVAL ESTIMATION USING LIMITED NUMBER OF RADIATION PATTERNS

The majority of publications involve 10 snapshots of test signal impinging the antenna from an unknown direction. Because the same number of snapshots has to be acquired for every radiation pattern, the number of ESPAR antenna radiation patterns directly influences the total number of snapshots required for DoA estimation. Therefore, it has direct implication on energy efficiency of battery powered IoT nodes.

The proposed low-profile ESPAR antenna has only 8 unique main beam directions but provides results at the similar DoA estimation accuracy levels as the high-profile ESPAR antenna having 12 unique main beam directions and the same energy-efficient simplified beam steering. In consequence, the proposed antenna gives the possibility to conduct DoA estimation approximately 33% faster when compared to the high-profile counterpart.

To further reduce the time needed for DoA estimation using our low-profile antenna, we propose to use lower number of radiation patterns than 8. To this end, we performed DoA estimation in the horizontal plane using power pattern cross-correlation (PPCC) algorithm (1) for three considered SNR

values, while the number of radiation patterns used in the estimation process was changing from 4 to 8. Results gathered in table 5, where specific radiation patterns from table 1 have been used for DoA estimation, indicate that it is possible to use only 4 patterns and still get acceptable results. Moreover, when 6 radiation patterns are used, the results do not significantly deteriorate form those obtained for 8 radiation patterns for all SNR levels. Therefore, the proposed antenna enables DoA estimation that is approximately 50% faster when compared to the high-profile ESPAR antenna with the same simplified beam steering.

TABLE 5. DoA estimation errors obtained for the proposed low-profile ESPAR antenna when only specific radiation patterns are used in PPCC algorithm (see text for explanations).

Radiation patterns used	SNR = 20 dB		SNR = 10 dB		SNR = 0 dB	
	RMS	prec.	RMS	prec.	RMS	prec.
[1 2 3 4 5 6 7 8]	0.85°	2°	1.32°	4°	2.52°	8°
[2 4 6 8]	1.29°	4°	2.92°	11°	4.19°	11°
[2 4 5 6 8]	1.19°	4°	1.43°	4°	3.35°	8°
[2 3 4 5 6 8]	0.95°	2°	1.49°	4°	2.92°	8°
[2 3 4 5 6 7 8]	0.82°	2°	1.48°	4°	2.76°	8°

TABLE 6. DoA estimation errors obtained using PPCC-MCP algorithm and limited number of radiation patterns of the proposed antenna (see text for explanations).

θ_t	SNR = 20 dB		SNR = 10 dB		SNR = 0 dB	
	RMS	prec.	RMS	prec.	RMS	prec.
10°	1.28°	5°	1.04°	2°	41.46°	179°
20°	0.85°	2°	1.27°	4°	2.30°	7°
30°	0.55°	2°	1.09°	2°	2.25°	6°
40°	0.83°	2°	0.85°	2°	2.15°	6°
50°	0.93°	2°	1.08°	3°	2.09°	4°
60°	0.82°	2°	1.61°	4°	29.43°	176°
70°	0.96°	2°	1.63°	4°	2.58°	8°
80°	0.78°	2°	1.11°	3°	2.40°	5°
90°	0.96°	2°	1.46°	4°	3.46°	13°
Cumul.	**0.90°**	**5°**	**1.26°**	**4°**	**17.09°**	**179°**

As a final verification of DoA estimation using limited number of low-profile ESPAR antenna's radiation patterns, a test using a BPSK signal coming from 36 horizontal directions within 9 elevation planes for three considered SNR values has been performed. Estimated DoA angles calculated using PPCC-MPC algorithm (2) and 6 radiation patterns, namely patterns number 2, 3, 4, 5, 6 and 8 from table 1, are shown in table 6. By comparing cumulative values of DoA estimation errors with those from table 4, it is clearly visible that 6 radiation patterns can be used for DoA estimation in IoT deployment scenarios, in which SNR do not exceed 10 *dB* providing similar results to those when 8 radiation patterns are used. Because, in noisy environments one may expect higher errors, future IoT nodes employing the proposed low-profile ESPAR antenna should have a certain level of adaptability and adjust the number of radiation patterns used for RSS-based DoA estimation as the overall SNR changes.

V. CONCLUSIONS

In the paper, new low-profile ESPAR antenna, that can be successfully used in RSS-based DoA estimation, has been presented. The proposed antenna has over 3 times lower height than high-profile ESPAR antenna designs currently available in the literature for DoA estimation, can provide 8 unique main beam directions and relies on simplified beam steering, which makes it applicable to simple and inexpensive IoT nodes. Measurements performed in our anechoic chamber using SDR-based setup and PPCC algorithm indicate that the overall DoA estimation accuracy achievable using the proposed antenna is similar to those available for high-profile ESPAR antenna having 12 unique main beam directions and relying on the similar energy-efficient simplified beam steering concept. Additionally, DoA error levels are low even in presence of high noise and, due to lower number of radiation patterns, for the proposed antenna it is possible to reduce the overall time required for DoA estimation by 33%. Therefore, the antenna can successfully be used in IoT nodes, in which the total height of the complete antenna has to be low, designed to be deployed in practical Smart City installations.

ACKNOWLEDGMENT

The authors would like to thank the editors and the anonymous reviewers for their suggestions and valuable comments that helped the authors to improve the overall quality and clarity of the paper.

The authors would like to thank the Academic Computer Centre in Gdansk, Poland (TASK) were all the calculations were carried out.

REFERENCES

[1] A. Zanella, N. Bui, A. Castellani, L. Vangelista, and M. Zorzi, "Internet of Things for smart cities," *IEEE Internet Things J.*, vol. 1, no. 1, pp. 22–32, Feb. 2014.

[2] F. Alam, R. Mehmood, I. Katib, N. N. Albogami, and A. Albeshri, "Data fusion and IoT for smart ubiquitous environments: A survey," *IEEE Access*, vol. 5, pp. 9533–9554, 2017.

[3] P. Sotres, J. R. Santana, L. Sánchez, J. Lanza, and L. Muñoz, "Practical lessons from the deployment and management of a smart city Internet-of-Things infrastructure: The SmartSantander testbed case," *IEEE Access*, vol. 5, pp. 14309–14322, 2017.

[4] A. Kausar, H. Mehrpouyan, M. Sellathurai, R. Qian, and S. Kausar, "Energy efficient switched parasitic array antenna for 5G networks and IoT," in *Proc. Loughborough Antennas Propag. Conf. (LAPC)*, Loughborough, U.K., Nov. 2016, pp. 1–5.

[5] R. F. Harrington, "Reactively controlled directive arrays," *IEEE Trans. Antennas Propag.*, vol. AP-26, no. 3, pp. 390–395, May 1978.

[6] K. Gyoda and T. Ohira, "Design of electronically steerable passive array radiator (ESPAR) antennas," in *Proc. IEEE Antennas Propag. Symp.*, Salt Lake City, UT, USA, vol. 2, Jul. 2000, pp. 922–925.

[7] R. Schlub and D. V. Thiel, "Switched parasitic antenna on a finite ground plane with conductive sleeve," *IEEE Trans. Antennas Propag.*, vol. 52, no. 5, pp. 1343–1347, May 2004.

[8] Ł. Kulas, "Direction-of-arrival estimation using an ESPAR antenna with simplified beam steering," in *Proc. 47th Eur. Microw. Conf.*, Nuremberg, Germany, Oct. 2017, pp. 296–299.

[9] E. Taillefer, C. Plapous, J. Cheng, K. Iigusa, and T. Ohira, "Reactance-domain MUSIC for ESPAR antennas (experiment)," in *Proc. IEEE Wireless Commun. Netw. Conf.*, New Orleans, LA, USA, vol. 1, Mar. 2003, pp. 98–102.

[10] E. Taillefer, A. Hirata, and T. Ohira, "Direction-of-arrival estimation using radiation power pattern with an ESPAR antenna," *IEEE Trans. Antennas Propag.*, vol. 53, no. 2, pp. 678–684, Feb. 2005.

[11] L. Kulas, "RSS-based DoA estimation using ESPAR antennas and interpolated radiation patterns," *IEEE Antennas Wireless Propag. Lett.*, vol. 17, no. 1, pp. 25–28, Jan. 2018.

[12] M. Donelli, F. Viani, P. Rocca, and A. Massa, "An innovative multiresolution approach for DOA estimation based on a support vector classification," *IEEE Trans. Antennas Propag.*, vol. 57, no. 8, pp. 2279–2292, Aug. 2009.

[13] F. Viani, L. Lizzi, M. Donelli, D. Pregnolato, G. Oliveri, and A. Massa, "Exploitation of parasitic smart antennas in wireless sensor networks," *J. Electromagn. Wave Appl.*, vol. 24, no. 7, pp. 993–1003, Jan. 2010.

[14] S. Chandran, Ed., *Advances in Direction-of-Arrival Estimation*. London, U.K.: Artech House, 2005.

[15] M. Rzymowski, P. Woznica, and L. Kulas, "Single-anchor indoor localization using ESPAR antenna," *IEEE Antennas Wireless Propag. Lett.*, vol. 15, pp. 1183–1186, 2016.

[16] A. Bensky, *Wireless Positioning Technologies and Applications*. Norwood, MA, USA: Artech House, 2007.

[17] S. Sugiura and H. Iizuka, "Reactively steered ring antenna array for automotive application," *IEEE Trans. Antennas Propag.*, vol. 55, no. 7, pp. 1902–1908, Jul. 2007.

[18] R. J. Dinger, "A planar version of a 4.0 GHz reactively steered adaptive array," *IEEE Trans. Antennas Propag.*, vol. AP-34, no. 3, pp. 427–431, Mar. 1986.

[19] E. Nishiyama, R. Hisadomi, and M. Aikawa, "Beam controllable microstrip antenna with switching diode," in *Proc. IEEE Antennas Propag. Symp.*, Albuquerque, NM, USA, Jul. 2006, pp. 2337–2340.

[20] W. Chen, J. Sun, X. Wang, and Z. Feng, "Design of planar ESPAR antenna by using sidelobe reduction algorithm," in *Proc. Microw. Millim. Wave Technol. (ICMMT)*, Apr. 2007, pp. 1–4.

[21] L. Zhang, S. Gao, Q. Luo, P. R. Young, and Q. Li, "Planar ultrathin small beam-switching antenna," *IEEE Trans. Antennas Propag.*, vol. 64, no. 12, pp. 5054–5063, Dec. 2016.

[22] T. Zhang, "A new planar electronically steerable passive array radiator antenna," in *Proc. 10th Int. Symp. Antennas, Propag. EM Theory*, Xi'an, China, Oct. 2012, pp. 1–3.

[23] J. Sun, W. Chen, X. Wang, Z. Feng, Y. Furuya, and A. Kuramoto, "Realization and measurements of planar switchable antenna system," in *Proc. Asia–Pacific Microw. Conf.*, Yokohama, Japan, Dec. 2006, pp. 339–342.

[24] H. Kato and Y. Kuwahara, "Novel ESPAR antenna," in *Proc. Antennas Propag. Soc. Int. Symp.*, vol. 4B, Jul. 2005, pp. 23–26.

[25] M. R. Kamarudin, P. S. Hall, F. Colombel, and M. Himdi, "Electronically switched beam disk-loaded monopole array antenna," *Prog. Electromagn. Res.*, vol. 101, pp. 339–347, 2010.

[26] S. Jeong, D. Ha, and W. J. Chappell, "A planar parasitic array antenna for tunable radiation pattern," in *Proc. IEEE Antennas Propag. Soc. Int. Symp.*, Jun. 2009, pp. 1–4.

[27] M. Rzymowski and L. Kulas, "Influence of ESPAR antenna radiation patterns shape on PPCC-based DoA estimation accuracy," in *Proc. 22nd Int. Conf. Microw., Radar Wireless Commun.*, Poznań, Poland, May 2018, pp. 69–72.

[28] K. Kaneta, T. Kondo, M. Ando, and N. Goto, "A flush-mounted antenna for mobile communications," in *Proc. IEEE AP-S Int. Symp., Antennas Propag.*, Syracuse, NY, USA, vol. 3, Jun. 1988, pp. 1323–1326.

[29] F. Zavosh and J. T. Aberle, "Improving the performance of microstrip-patch antennas," *IEEE Antennas Propag. Mag.*, vol. 38, no. 4, pp. 7–12, Aug. 1996.

[30] N. C. Karmakar, "Investigations into a cavity-backed circular-patch antenna," *IEEE Trans. Antennas Propag.*, vol. 50, no. 12, pp. 1706–1715, Dec. 2002.

[31] M. Plotka, M. Tarkowski, K. Nyka, and L. Kulas, "A novel calibration method for RSS-based DoA estimation using ESPAR antennas," in *Proc. 22nd Int. Conf. Microw., Radar Wireless Commun.*, Poznań, Poland, 2018, pp. 65–68.

[32] Q. Hou, H. Tang, Y. Liu, and X. Zhao, "Dual-frequency and broadband circular patch antennas with a monopole-type pattern based on epsilon-negative transmission line," *IEEE Antennas Wireless Propag. Lett.*, vol. 11, pp. 442–445, 2012.

[33] R. Garg, P. Bhartia, I. Bahl, and A. Ittipiboon, *Microstrip Antenna Design Handbook*. Boston, MA, USA: Artech House, 2001.

[34] D. Schaubert, F. Farrar, A. Sindoris, and S. Hayes, "Microstrip antennas with frequency agility and polarization diversity," *IEEE Trans. Antennas Propag.*, vol. AP-29, no. 1, pp. 118–123, Jan. 1981.

[35] J. S. Dahele and K. F. Lee, "Theory and experiment on microstrip antennas with airgaps," *IEE Proc. H-Microw., Antennas Propag.*, vol. 132, no. 7, pp. 455–460, Dec. 1985.

[36] M. Jusoh, T. Sabapathy, M. F. Jamlos, and M. R. Kamarudin, "Reconfigurable four-parasitic-elements patch antenna for high-gain beam switching application," *IEEE Antennas Wireless Propag. Lett.*, vol. 13, pp. 79–82, 2014.

[37] M. S. Alam and A. M. Abbosh, "Beam-steerable planar antenna using circular disc and four pin-controlled tapered stubs for WiMAX and WLAN applications," *IEEE Antennas Wireless Propag. Lett.*, vol. 15, pp. 980–983, 2016.

[38] S. J. Shi and W. P. Ding, "Radiation pattern reconfigurable microstrip antenna for WiMAX application," *Electron. Lett.*, vol. 51, no. 9, pp. 662–664, 2015.

[39] M. Rzymowski and L. Kulas, "RSS-based direction-of-arrival estimation with increased accuracy for arbitrary elevation angles using ESPAR antennas," in *Proc. 12th Eur. Conf. Antennas Propag. (EuCAP)*, London, U.K., 2018, pp. 1–4.

[40] M. Groth and L. Kulas, "Accurate PPCC-based DoA estimation using multiple calibration planes for WSN nodes equipped with ESPAR antennas," in *Proc. 48th Eur. Microw. Conf. (EuMW)*, Madrid, Spain, Sep. 2018, pp. 1565–1568.

MATEUSZ BURTOWY received the B.Sc. and M.Sc. degrees in microwave engineering from the Gdańsk University of Technology, Gdańsk, Poland, in 2014 and 2016, respectively. He is currently an Antenna Designer with PIT-RADWAR S.A and, simultaneously, continues his research activities at Gdańsk University of Technology. His main interests include antenna design and radar techniques.

MATEUSZ RZYMOWSKI received the M.Sc. degree in microwave engineering from the Gdańsk University of Technology, Gdańsk, Poland, in 2010, where he is currently a Researcher with the Department of Microwave and Antenna Engineering, organizing and conducting research for EU companies within EU-funded research and development projects. His main interests include reconfigurable antennas, millimeter wave antenna design, and security mechanisms that can be implemented in the physical layer of wireless systems.

LUKASZ KULAS received the M.Sc. and Ph.D. degrees (Hons.) in microwave engineering from the Gdańsk University of Technology, Gdańsk, Poland, in 2001 and 2007, respectively, where he is currently an Assistant Professor with the Department of Microwave and Antenna Engineering. He actively cooperates with EU industry within a numerous research and development projects. His main interests are reconfigurable antennas, direction-of-arrival algorithms, wireless embedded devices, and the Internet-of-Things solutions that can be applied in practical industrial applications.